

# Transparent, luminescent terbium doped zirconia: development of optical-structural ceramics with integrated temperature measurement functionalities

C. L. Hardin,<sup>1</sup> Y. Kodera,<sup>1</sup> S. A. Basun,<sup>2</sup> D. R. Evans,<sup>2</sup> and J. E. Garay<sup>1,\*</sup>

<sup>1</sup>Department of Mechanical Engineering and Materials Science and Engineering Program, University of California Riverside, Riverside, CA 92521, USA

<sup>2</sup>Air Force Research Laboratory, Materials and Manufacturing Directorate, WPAFB, OH 45433, USA  
[\\*jegaray@enr.ucr.edu](mailto:*jegaray@enr.ucr.edu)

**Abstract:** We present a method for the preparation of transparent Tb doped zirconia (Tb:ZrO<sub>2</sub>) ceramics that luminesce in the visible. The visible luminescence is temperature dependent, yielding samples that have integrated temperatures sensing capabilities. Our approach is to simultaneously react and densify ZrO<sub>2</sub> and Tb<sub>4</sub>O<sub>7</sub> using current activated pressure assisted densification (CAPAD). The Tb dopant serves to both stabilize the tetragonal phase of zirconia and for emitting light. The Tb:ZrO<sub>2</sub> ceramics have an excellent combination of structural and optical properties; the toughness is comparable to yttria stabilized zirconia and the transparency in the visible is high. Moreover, the luminescent lifetimes are long and amenable to luminescent thermometry. The ceramics have promise as thermal barrier materials and high-strength windows with “built-in” temperature measurement capabilities.

©2013 Optical Society of America

**OCIS codes:** (160.2540) Fluorescent and luminescent materials; (160.4236) Nanomaterials; (160.4670) Optical materials; (160.5690) Rare-earth-doped materials.

---

## References and links

1. S. Ghosh, D. Teweldebrhan, J. R. Morales, J. E. Garay, and A. A. Balandin, “Thermal properties of the optically transparent pore-free nanostructured yttria-stabilized zirconia,” *J. Appl. Phys.* **106**(11), 113507 (2009).
2. J. E. Alaniz, F. G. Perez-Gutierrez, G. Aguilar, and J. E. Garay, “Optical properties of transparent nanocrystalline yttria stabilized zirconia,” *Opt. Mater.* **32**(1), 62–68 (2009).
3. S. R. Casolco, J. Xu, and J. E. Garay, “Transparent/translucent polycrystalline nanostructured yttria stabilized zirconia with varying colors,” *Scr. Mater.* **58**(6), 516–519 (2008).
4. E. H. Penilla, Y. Kodera, and J. E. Garay, “Simultaneous synthesis and densification of transparent, photoluminescent polycrystalline YAG by current activated pressure assisted densification (CAPAD),” *Mater. Sci. Eng. B* **177**(14), 1178–1187 (2012).
5. A. T. Wieg, Y. Kodera, Z. Wang, T. Imai, C. Dames, and J. E. Garay, “Visible photoluminescence in polycrystalline terbium doped aluminum nitride (Tb:AlN) ceramics with high thermal conductivity,” *Appl. Phys. Lett.* **101**(11), 111903 (2012).
6. M. D. Chambers and D. R. Clarke, “Doped oxides for high-temperature luminescence and lifetime thermometry,” *Annu. Rev. Mater. Res.* **39**(1), 325–359 (2009).
7. M. M. Gentleman and D. R. Clarke, “Luminescence sensing of temperature in pyrochlore zirconate materials for thermal barrier coatings,” *Surf. Coat. Tech.* **200**(5-6), 1264–1269 (2005).
8. Y. Shen, M. D. Chambers, and D. R. Clarke, “Effects of dopants and excitation wavelength on the temperature sensing of Ln<sup>3+</sup>-doped 7YSZ,” *Surf. Coat. Tech.* **203**(5-7), 456–460 (2008).
9. M. D. Chambers and D. R. Clarke, “Terbium as an alternative for luminescence sensing of temperature of thermal barrier coating materials,” *Surf. Coat. Tech.* **202**(4-7), 688–692 (2007).
10. S. Gutzov and W. Assmus, “The luminescence of holmium doped cubic yttria-stabilized zirconia,” *J. Mater. Sci. Lett.* **19**(4), 275–277 (2000).
11. Y. Kodera, C. L. Hardin, and J. E. Garay, “Transmitting, emitting and controlling light: processing of transparent ceramics using current activated pressure assisted densification,” *Scr. Mater.* (to be published).

12. J. E. Garay, "Current activated pressure assisted densification of materials," *Annu. Rev. Mater. Res.* **40**(1), 445–468 (2010).
  13. K. Niihara, R. Morena, and D. Hasselman, "Evaluation of K<sub>1c</sub> of brittle solids by the indentation method with low crack-to-indent ratios," *J. Mater. Sci.* **1**, 13–16 (1982).
  14. G. Anstis, P. Chantikul, B. R. Lawn, and D. B. Marshall, "A critical evaluation of indentation techniques for measuring fracture toughness: I, direct crack measurements," *J. Am. Ceram. Soc.* **64**(9), 533–538 (1981).
  15. R. P. Ingel and D. Lewis III, "Lattice parameters and density for Y<sub>2</sub>O<sub>3</sub>-stabilized ZrO<sub>2</sub>," *J. Am. Ceram. Soc.* **69**(4), 325–332 (1986).
  16. P. Manning, J. Sirman, R. De Souza, and J. Kilner, "The kinetics of oxygen transport in 9.5 mol% single crystal yttria stabilised zirconia," *Solid State Ion.* **100**(1-2), 1–10 (1997).
  17. V. B. Vykhodets, T. E. Kurennykh, G. Kesarev, M. V. Kuznetsov, V. V. Kondrat'ev, C. Hülsen, and U. Koester, "Diffusion of insoluble carbon in zirconium oxides," *JETP Lett.* **93**(1), 5–9 (2011).
  18. M. Kilo, M. A. Taylor, C. Argiris, G. Borchardt, B. Lesage, S. Weber, S. Scherrer, H. Scherrer, M. Schroeder, and M. Martin, "Cation self-diffusion of <sup>44</sup>Ca, <sup>88</sup>Y, and <sup>90</sup>Zr in single-crystalline calcia- and yttria-doped zirconia," *J. Appl. Phys.* **94**(12), 7547–7552 (2003).
  19. J. Klimke, M. Trunec, and A. Krell, "Transparent tetragonal yttria-stabilized zirconia ceramics: influence of scattering caused by birefringence," *J. Am. Ceram. Soc.* **94**(6), 1850–1858 (2011).
  20. G. H. Dieke, *Spectra and Energy Levels of Rare Earth Ions in Crystals* (Interscience, 1968).
- 

## 1. Introduction

Stabilized zirconium oxide (zirconia) is one of the most technologically important and widely used structural ceramics due to its excellent thermal stability, low thermal conductivity (important for thermal barrier applications) [1] and high fracture toughness. Despite its widespread use, polycrystalline zirconia is not usually thought of as a material suitable for optical applications because it is usually opaque. Some recent studies however, have shown that with careful control of the microstructure, zirconia can be reliably made transparent [2,3], yielding a versatile optical-structural ceramic.

Luminescent functionalization of ceramics through rare earth (RE) doping has also attracted considerable attention lately. There is interest in RE-doped ceramics for solid state lighting [4], laser host materials [5] and for luminescence thermometry [6]. The latter application is particularly interesting for zirconia, since partially stabilized zirconia is common in high temperature structural applications such as protective coatings in jet turbine engines [6]. Luminescence thermometry takes advantage of the temperature dependent photoluminescence of rare earth ions to measure the temperature of the ceramic part. One of the major advantages of this phenomenon is that it does not require contact, which makes it possible to determine temperature of moving parts.

Successful demonstrations of luminescent RE doping of zirconia have been presented by different groups [7–10]. In these studies the approach was to add a small amount of luminescent RE (Ho, Er, Sm, *etc.*) as well as yttrium. The RE serves for the luminescence functionality while the Y is for stabilizing the tetragonal phase. These studies confirm that luminescence provides a valuable integrated measurement scheme in zirconia. Chambers and Clarke [6,9] point out that Tb is an ideal dopant because it emits in the blue-green end of spectrum making it sensitive at higher temperatures where the back-ground radiation is high. However attempts to produce Tb doped luminescent polycrystalline zirconia by sintering were unsuccessful [9], likely because of the formation of Tb<sup>4+</sup> rather than Tb<sup>3+</sup> which is the ion that luminesces under the desired conditions.

An alternative to free sintering is current activated pressure assisted densification (CAPAD). Although CAPAD has been used recently to produce a wide variety of transparent ceramics, most of the work has been done on cubic (optically isotropic) ceramics that do not luminesce [11]. Here we present a method for producing tetragonal zirconia ceramics with good transparency that also luminesces in the visible. We used CAPAD to simultaneously react and densify zirconia and terbium powders. In contrast to previous work we use only one rare earth additive, Tb (rather than a combination of RE and Y) that serves to both stabilize the zirconia and provide visible luminescence. Furthermore we concentrated on producing tetragonal zirconia since it has superior mechanical properties compared to cubic zirconia.

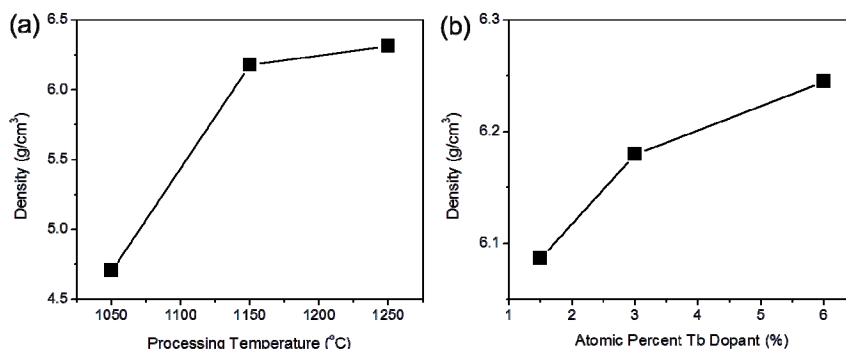


Fig. 1. The effect of (a) processing temperature and (b) Tb dopant concentration on the bulk density of Tb:ZrO<sub>2</sub>. A fixed Tb concentration (3%Tb:ZrO<sub>2</sub>) was used for all samples in (a) and constant processing temperature of 1150° C was used in (b) (lines between points are guide to eye only).

## 2. Experimental procedure

### 2.1. Powder preparation and CAPAD processing

Commercially pure non-doped ZrO<sub>2</sub> (Tosoh Corporation), Tb<sub>4</sub>O<sub>7</sub> (NanoAmor, 99.995% purity, 46-60 nm size), Y<sub>2</sub>O<sub>3</sub> (Inframat Advanced Materials, 99.95% purity, 30-50nm) were used to make the reaction-densified ceramics. We also prepared ceramics using pre-doped yttria powder (Tosoh Corporation TZ-3Y-E, ~50nm grain size). Each powder was weighed to generate the appropriate stoichiometry. The powders were then mixed manually using a mortar and pestle to obtain macro scale mixing of the powders. The powder was then mixed in a low energy ball mill in a glass jar using a 20:1 ball to powder ratio of 5 mm ZrO<sub>2</sub> grinding balls. The powder was then mixed manually in the mortar pestle again in order to break down any agglomerates formed in the low energy ball mill. Dopant levels were chosen in order to study the effects of the dopant both on the structural stabilization of the zirconia as well as the effects on optical and luminescent properties.

The mixed powder was loaded into a graphite die between two 19 mm graphite punches and processed using our CAPAD apparatus which has been described before [12]. The chamber was then evacuated to a pressure of  $3 \times 10^{-2}$  Torr. Then the sample was pre-pressed at a pressure of 70 MPa for 1 minute to break down agglomerates and make a more dense green body. The sample was then simultaneously heated to an intermediate temperature of ~550°C and loaded to a pressure of 104 MPa over a 3 minute period. At this point the sample was heated at 200°C/min to the desired processing temperature and held to a total experiment time of 15 minutes at which point the current and load were released.

### 2.2. Microstructural and structural characterization

The as-produced samples were removed from the die and mechanically polished to uniform thickness. Density of the samples was measured via Archimedes method utilizing a Mettler-Toledo XS104 scale with density measurement accessory. Samples were then analyzed using a Philips XL30-FEG SEM using both secondary electron (SE) and back-scattered electron (BSE) detectors to ensure phase uniformity. Pieces of the sample were broken off for fracture surface SE analysis to determine average grain size of the samples. Samples were characterized using a Bruker D8 powder XRD as well as a Horiba LabRam micro-Raman for phase analysis. Samples were mechanically tested using a Wilson Tukon 2100 hardness tester using a Vickers indenter. Hardness values were measured using 2 kg and fracture toughness was measured using a 5 kg load. Fracture toughness,  $K_{IC}$  values were calculated using both the Niihara [13] and Anstis [14] equations.

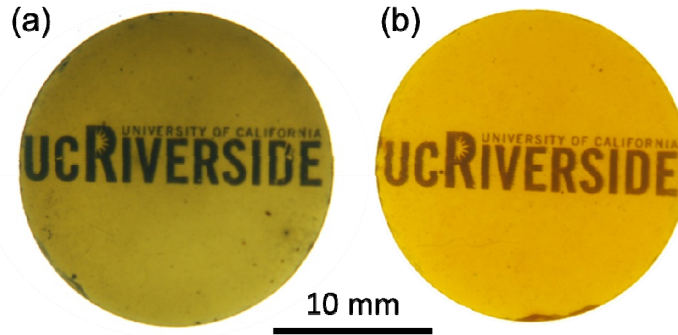


Fig. 2. Photographs of a 6%Tb:ZrO<sub>2</sub> samples on the top of backlit text, demonstrating transparency. (a) as-processed sample. (b) sample annealed at 700° C for 24 hrs.

### 2.3. Optical characterization

The optical transmission of the samples were measured using a CARY 50 UV/VIS spectrometer. Steady state photoluminescence properties were measured using a Horiba Spex Fluorolog spectrophotometer. Photoluminescence decay measurements were made using the fourth harmonic of an ND:YAG laser (266 nm wavelength) and an Oriel Instruments Cornerstone 260 ¼ meter monochromator with an Oriel 77341 photomultiplier tube.

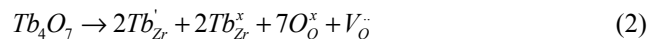
### 3. Results and discussion

Figure 1a shows sample density vs. processing temperature for Tb:ZrO<sub>2</sub> samples with 3% Tb while Fig. 1b shows the effect of varying Tb dopant concentration while holding the processing temperature constant at 1150°C. As expected, the density of samples increases with processing temperature, because of higher densification (less porosity). The density of the samples is similar at temperatures above 1150 °C. The amount of Tb dopant also plays a role; the density increases with higher Tb content. This trend of increasing density is opposite to what is seen with Ytria stabilization.

R. P. Ingel et al. [15] studied the effect of Y<sub>2</sub>O<sub>3</sub> concentration on the density of YSZ. They report that the measured and calculated density of the YSZ decreases as the Y<sub>2</sub>O<sub>3</sub> content is increased. For example, the calculated polycrystalline densities of YSZ were 6.16, 6.12 and 6.02 g/cm<sup>3</sup> when the concentrations of doped Y<sub>2</sub>O<sub>3</sub> were 0, 1.5 and 6%, respectively. This dependence is caused by the increase in the charge compensating vacancies generated due to the different valence states of Zr<sup>4+</sup> and Y<sup>3+</sup>. This incorporation of Y<sub>2</sub>O<sub>3</sub> into ZrO<sub>2</sub> causing the formation of vacancies for charge compensation can be written in Kroger-Vink notation as:



By contrast Tb can be Tb<sup>3+</sup> or Tb<sup>4+</sup> as indicated by the Tb<sub>4</sub>O<sub>7</sub> stoichiometry. However, the doping of Tb which in Tb<sub>4</sub>O<sub>7</sub> is effectively half Tb<sup>3+</sup> and Tb<sup>4+</sup> would still require charge compensation. One possibility is:



Thus it is not likely that lack of vacancy formation is responsible for the increase in density with increasing Tb content observed in Fig. 1b. Instead the differing trend is likely due to the difference in atomic mass of Tb and Y. Increasing dopant concentration into ZrO<sub>2</sub> effects not only the lattice parameter and the crystal structure but also the overall molar mass. The relative atomic mass of Y is 88.91, compared to Tb which is 158.93 and about 1.8 times that of Zr (91.22). This effect of the mass difference could be responsible for the Tb content dependence that we observe being opposite to traditionally observed for Y. Although we cannot calculate the relative density or porosity concentration due to the lack of information

on the theoretical density of Tb stabilized zirconia, the porosity of the samples should be very low as evidenced by high transparency of the samples as will be discussed below.

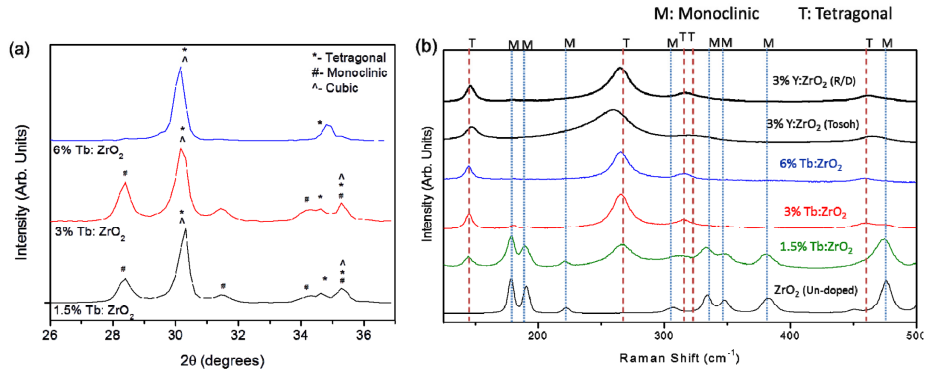


Fig. 3. X-ray diffraction profiles of Tb:ZrO<sub>2</sub> samples with varying Tb content (a) and Raman spectra of Tb:ZrO<sub>2</sub> samples with varying Tb content (b).

Figure 2 are pictures of a 6% Tb:ZrO<sub>2</sub> ceramic placed on printed text on a light table. Figure 2a is the as-processed sample while Fig. 2b is the same sample after annealing in air at 700 °C for 24 hours. Comparison of the pictures reveals that annealing in air changes the color of the sample; this effect will be discussed in detail below. The text is legible through the sample, confirming the high densities and transparency of our samples.

It is well known that depending on the degree of stabilizing dopant (often Ca or Y) zirconia can be monoclinic, tetragonal or cubic. Figure 3 shows XRD (a) and Raman (b) spectra for zirconia samples produced with varying atomic percent Tb. For comparison, we also plotted Raman spectra for a non-doped ZrO<sub>2</sub> and two Y doped samples. One Y:ZrO<sub>2</sub> was made using the identical reaction/densification process as the Tb:ZrO<sub>2</sub>, while another was made using commercially available pre-doped powder; we refer to the samples as 3% Y:ZrO<sub>2</sub> (R/D) and 3% Y:ZrO<sub>2</sub> (Tosoh), respectively. The results reveal that as the dopant level is

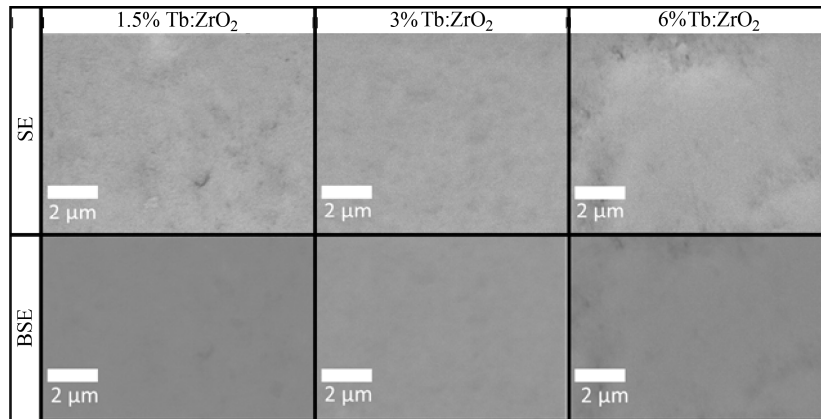


Fig. 4. Secondary Electron (SE) and Backscatter Electron (BSE) micrographs for Tb:ZrO<sub>2</sub> samples with varying Tb content.

increased, the structure of the samples changes from a pure monoclinic structure, as shown in the undoped sample, to a purely tetragonal phase as shown in the 6% Tb:ZrO<sub>2</sub> sample. The 1.5% and 3% Tb:ZrO<sub>2</sub> samples contain both monoclinic and tetragonal phases. These results confirm that Tb can serve to stabilize the tetragonal phase in zirconia. The Raman spectra of

the as reaction/densified 3% Y:ZrO<sub>2</sub> is very similar to the 3% Tb:ZrO<sub>2</sub>, while the peak at ~260 cm<sup>-1</sup> is more asymmetric in the 3% Y:ZrO<sub>2</sub> sample made with pre-reacted commercial powder. Since Tb and Y can both be trivalent, it is likely that the stabilization mechanism is similar to Y stabilization.

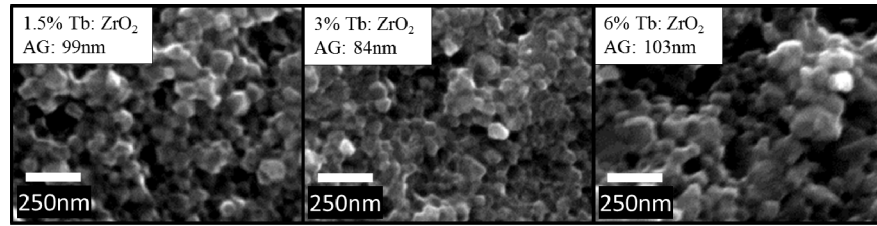


Fig. 5. SEM micrographs of fracture surfaces of Tb:ZrO<sub>2</sub> with varying dopant levels.

SEM micrographs of polished surfaces of Tb:ZrO<sub>2</sub> with varying atomic percent Tb using both secondary electron (SE) and back-scattered electron (BSE) detectors are shown in Fig. 4. The micrographs show high phase uniformity and no dopant segregation. The lack of observable phase segregation suggests that the Tb ions have been incorporated into the ZrO<sub>2</sub> lattice, corroborating the Raman and XRD results which show that the Tb stabilizes the tetragonal phase.

Figure 5 are SEM micrographs of fracture surfaces of the same samples shown in Fig. 4, showing average grain sizes varying between 84 and 103nm. The fine grain sizes of the Tb:ZrO<sub>2</sub> samples produced by our reaction/densification method promise good optical and structural properties as will be discussed below.

Figure 6 shows hardness and toughness measurements for both Tb and Y doped zirconia samples processed under identical conditions at 1150 °C. We chose to use both the Anstis and Niihara equations to calculate toughness, to facilitate comparison with previous work. The Tb:ZrO<sub>2</sub> ceramics compare favorably with traditional yttria doped samples; the Y:ZrO<sub>2</sub> sample shows slightly higher hardness and slightly lower toughness values than same concentration Tb doped samples. The hardness of Tb:ZrO<sub>2</sub> samples increases fairly linearly with dopant percentage. The fracture toughness ranges from 3.5 to almost 7 MPa/m<sup>0.5</sup> and is maximized at 3% Tb which is expected, since at this concentration the sample contains a mixture of tetragonal and monoclinic phases (see Fig. 3). These are high fracture toughness values for a ceramic and confirm that Tb:ZrO<sub>2</sub> ceramics are suitable for structural applications.

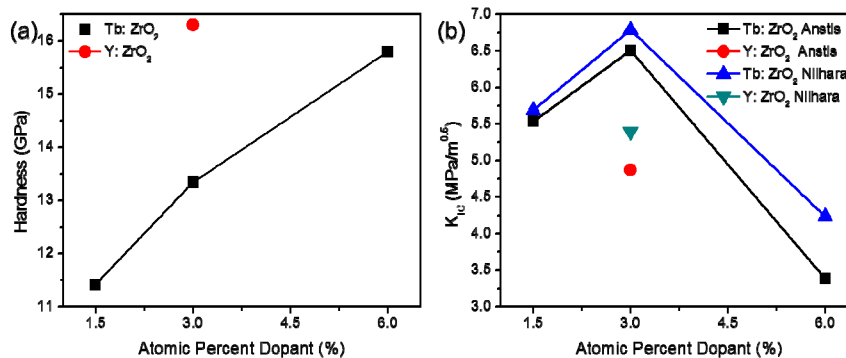


Fig. 6. Hardness and Toughness of ZrO<sub>2</sub> vs. Dopant Level (Y or Tb). Lines between points are guide to eye only.

It has been shown that oxygen vacancies play an important role in the optical properties of YSZ [2,11]. Specifically oxygen vacancies in zirconia have a positive charge so they can trap electrons, forming a color center that absorbs light in the visible. In Kroger-Vink notation an oxygen vacancy with a trapped electron can be written:



We believe we observe a similar effect in Tb:ZrO<sub>2</sub>. As seen in Fig. 2, the color of our samples change significantly during annealing. In order to better understand this effect, we performed a series of experiments to determine the effects of annealing on the optical properties of Tb:ZrO<sub>2</sub>. A 6% Tb:ZrO<sub>2</sub> was processed via CAPAD, polished, then annealed for up to 6 hours at 700 °C in a box furnace in air. The sample was polished and optical transmittance was measured. Figure 7a shows the effect of annealing in the presence of

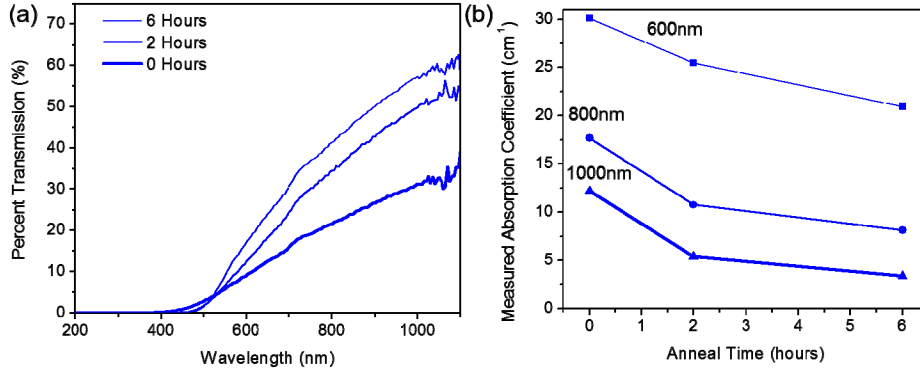


Fig. 7. Effect of annealing on the (a) optical transmission and (b) absorption coefficients of 6% Tb:ZrO<sub>2</sub>. (lines between points in (b) are guide to eye only).

oxygen on the transmission for various anneal times and wavelengths. The transmission data was also used to calculate absorption coefficients using Beer's Law:

$$T = (1 - R)^2 e^{-\beta l} \quad (4)$$

where  $l$  is the sample thickness,  $T$  is transmittance,  $R$  for reflectance, and  $\beta$  is the absorption coefficient. The reflectance was calculated using the refractive index,  $n$  of YSZ ( $n = 2.2$ ). These data are plotted vs. anneal time in Fig. 8b; the data reveal that the absorption coefficient decreases with annealing time for all wavelengths.

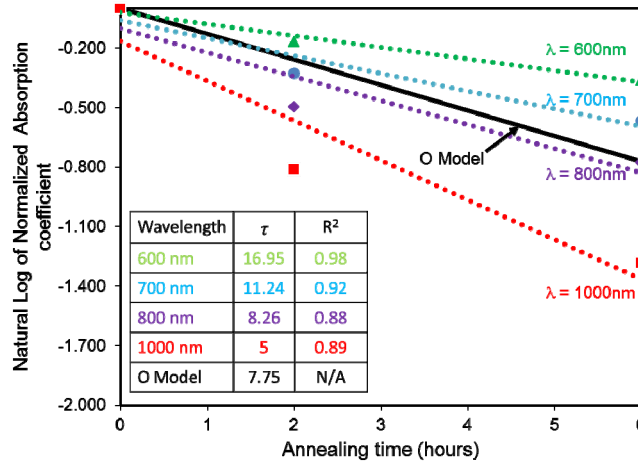


Fig. 8. Measured absorption coefficients for Tb:ZrO<sub>2</sub> compared to Oxygen diffusion model. The inset tabulates the relaxation time,  $\tau$  and  $R^2$  (for fit to exponential) for various wavelengths.

It is likely that the decrease in  $\beta$  can be attributed to a decreased concentration of vacancies with trapped electrons,  $[V_o^-]$  as defined by Eq. (1). Assuming a proportional relationship between absorption coefficient and vacancy concentration, we can write:

$$\beta \propto [V_o^-] \quad (5)$$

We can check the validity of the assumption that  $\beta$  is affected by vacancy concentration (and therefore oxygen diffusion) by applying an analytical diffusion model. Using Fick's second law for slab geometry with an initial vacancy concentration,  $[V_o^-]_0$  the time dependent average concentration of oxygen vacancies,  $[\overline{V_o^-}]$  is given by:

$$[\overline{V_o^-}](t) = \frac{1}{h} \int_0^h [V_o^-](x, t) dx = \frac{8[V_o^-]_0}{\pi^2} \sum_{j=0}^{\infty} \frac{1}{(2j+1)^2} \exp\left(-\left[\frac{(2j+1)\pi}{h}\right]^2 Dt\right) \quad (6)$$

where  $h$  is the thickness of the slab and  $D$  is the diffusion coefficient. A good approximation to Eq. (6) is

$$\frac{[\overline{V_o^-}]}{[V_o^-]_0} = \frac{8}{\pi^2} \exp\left(-\frac{t}{\tau}\right) \quad (7)$$

where the relaxation time,  $\tau$  is

$$\tau = \frac{h^2}{\pi^2 D} \quad (8)$$

Equation (8) reveals that the relaxation time is a function of the diffusivity,  $D$  of the diffusing species; the higher the diffusivity the shorter the relaxation time. Figure 8 is a plot of the natural log of

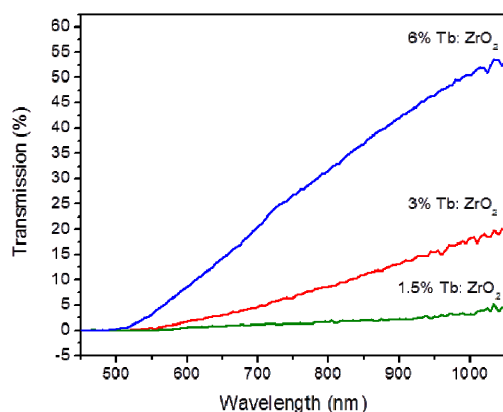


Fig. 9. Optical Transmission vs. Wavelength for Varying dopant content in Tb:ZrO<sub>2</sub>.

normalized absorption coefficient vs. anneal time. Absorption coefficients for each wavelength were normalized to the corresponding maximum value for each wavelength. The dashed lines are fits of the experimental points. The  $R^2$  values of the fits are shown in the inset for each of the wavelength. They range from 0.98 for 600 nm light to 0.89 for light in the near-IR (1000 nm). This good fit suggests that the absorption coefficients decay exponentially with time as in Eq. (7). Also plotted in Fig. 8 is a curve calculated using previously measured oxygen volume diffusivity [16] at the same temperature (700 °C), i.e. by using  $D$  from the literature directly into Eqs. (7) and (8). The slopes of the lines in Fig. 8 (corresponding to  $1/\tau$ ) are quite similar. The measured values for  $\tau$  at various wavelengths are reported in the inset

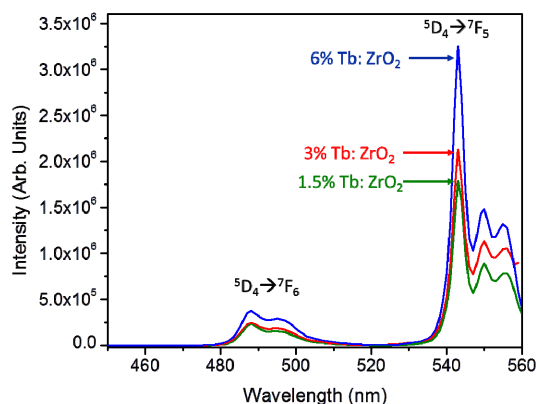


Fig. 10. Photoluminescence Spectra vs. wavelength for varying atomic percent Tb in Tb:ZrO<sub>2</sub> (290nm Excitation).

along with calculated values using oxygen diffusion. At all wavelengths the measured  $\tau$  is close to the  $\tau$  calculated for oxygen diffusion (within a factor of 2). By contrast, the corresponding time constants calculated using carbon diffusivity in zirconia [17] and zirconium volume diffusivity in zirconia [18] are  $1 \times 10^{13}$  and  $2.5 \times 10^{13}$  respectively—13 orders of magnitude higher than our measured relaxation times. The similarity of our measured relaxation time and that time constant calculated using oxygen diffusion data strongly suggest that the observed

effect of annealing time on  $\beta$  of Tb:ZrO<sub>2</sub> is related to the average oxygen vacancy concentration,  $\left[\overline{V}_o\right]$  changing as oxygen diffuses back into the oxygen deficient ceramics.

Figure 9 shows optical transmission of samples vs. atomic percent Tb. Sample transmission increases greatly with atomic percent Tb. We observe a transmission of <5% at 1 $\mu$ m for a 1.5% Tb sample vs. >50% transmission at 1 $\mu$ m for 6% Tb:ZrO<sub>2</sub>. It has been shown that light transmission increases with decreasing grain size in birefringent ceramics [11,19]. However, since the average grain size of our Tb:ZrO<sub>2</sub> is similar at all Tb concentrations

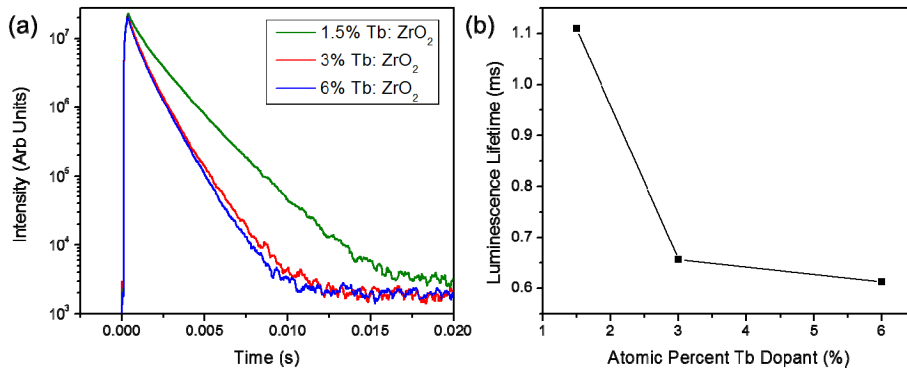


Fig. 11. Photoluminescence Decay vs. Dopant Level (15 point moving average applied to (a) for clarity), lines between points in (b) are guide to eye only).

(Fig. 5) it is not likely the differences in transparency as a function of Tb content we observe is caused by differing grain size. Instead we feel that the observed differences are caused by different refractive indices of the tetragonal and monoclinic phases (causing an effective birefringence). Klimke *et al.* surveyed available data on the birefringence ( $\Delta n$ ) of tetragonal YSZ and showed that the apparent ( $\Delta n$ ) can vary significantly between 0.2 to 0.9 [19]. It should be noted that these values even on the low end are higher than for hexagonal alumina ( $\Delta n = 0.008$ ), making producing tetragonal zirconia particularly difficult. The low transparency we observe at lower Tb content is likely due to high effective birefringence caused by the existence of monoclinic and tetragonal zirconia (Fig. 3).

Klimke *et al.* [19] also provided calculations based on Mie theory that fit well with experimental data. A similar analysis is not possible for our samples since the Mie scattering theory neglects absorption which is very important in our Tb:ZrO<sub>2</sub> samples as shown in Figs. 2 and 7. It is worth emphasizing that the optical transparency of the tetragonal 6%Tb:ZrO<sub>2</sub> is over 50% at 1 $\mu$ m. We attribute the high transparency of the 6%Tb:ZrO<sub>2</sub> samples to high density, small grain size and thus relatively low effect of birefringence.

The luminescent properties of the Tb doped samples were also investigated. Figure 10 shows photoluminescence spectra for varying atomic percent Tb under 290 nm excitation. All three dopant levels show sharp luminescence peaks, with intensities that increase with Tb concentration. The peaks correspond to the Tb<sup>3+</sup> transitions expected from the Dieke diagram [20]; the <sup>5</sup>D<sub>4</sub>→<sup>7</sup>F<sub>6</sub> centered around 500 nm and the <sup>5</sup>D<sub>4</sub>→<sup>7</sup>F<sub>5</sub> transition centered around 550 nm. As mentioned before, Tb ions are multivalent and can be Tb<sup>3+</sup> or Tb<sup>4+</sup>. The peaks in the luminescent spectra (Fig. 10) confirm the existence of Tb<sup>3+</sup> in Tb:ZrO<sub>2</sub> fabricated using the CAPAD method. It is worth emphasizing that previous attempts to produce luminescent Tb:ZrO<sub>2</sub> using conventional sintering did not succeed [1]. The lack of success was attributed to the formation of primarily Tb<sup>4+</sup>.

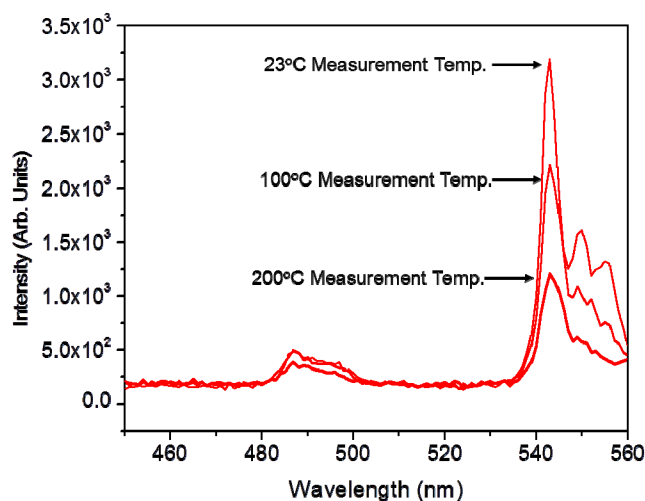


Fig. 12. Effect of measurement temperature on photoluminescence intensity for 3% Tb:ZrO<sub>2</sub>.

The amount of Tb concentration affected the luminescence decay as well (Fig. 11a). The 1.5% Tb:ZrO<sub>2</sub> shows a significantly longer luminescence lifetime (1.11 ms) than the 3% (0.613 ms) and 6% (0.657ms) samples as seen in Fig. 11b. This shorter lifetime is indicative of dopant quenching at higher levels of Tb doping. The temperature dependence of luminescence intensity is reported in Fig. 12, which shows the change in luminescence spectra vs. temperature for measurement temperatures ranging from 23°C to 200°C. Detectable changes in luminescent intensity with temperature suggest that Tb:ZrO<sub>2</sub> can be used in temperature sensing applications. Although the lifetime of luminescence is known to be a more sensitive temperature probe than intensity [6] we do not have temperature dependent lifetime measurement at this time. However we expect the lifetimes to show temperature dependence and are currently investigating this possibility.

#### 4. Summary

In summary, we have presented a method for producing transparent, luminescent Tb:ZrO<sub>2</sub> ceramics using CAPAD. The ceramics have a high fracture toughness values and confirm that Tb:ZrO<sub>2</sub> ceramics could be used for structural applications. The optical transparency can be influenced by annealing in air and an analytical model of oxygen diffusion fits well with our experimental results suggesting that the absorption coefficient,  $\beta$  of Tb:ZrO<sub>2</sub> is related to the average oxygen vacancy concentration,  $\left[ \overline{V_o} \right]$ . The luminescent intensity and lifetime depend on Tb content. In addition the luminescent lifetimes are long and the luminescent intensity is influenced by temperature suggesting that the ceramics can be used in a wide range of applications such as temperature sensitive transparent armor, windows, or thermal barriers.

#### Acknowledgments

Partial support of this work by the National Science Foundation (NSF Grant# DMR 0956071) is gratefully acknowledged.